NODE LOCATION OPTIMIZATION AND INQUIRY INTO GEOMETRY-PRESERVING VERSUS ISOPARAMETRIC FORMULATION IN THE COLLOCATION BOUNDARY ELEMENT METHOD

NEY AUGUSTO DUMONT
Department of Civil and Environmental Engineering, Pontifical Catholic University of Rio de Janeiro, Brazil

ABSTRACT

This paper might have a subtitle, '– homothetic node and element generation along boundary patches', with the justification 'to simplify and speed up the numerical simulation'. We have recently laid down the theoretical basis for the consistent formulation of the collocation boundary element method, as it should have been conceived from the beginning. We proposed a convergence theorem for two- and three-dimensional problems of elasticity and potential, which applies to arbitrarily curved elements in the frame of an isoparametric analysis. We also showed that arbitrarily high precision and accuracy may be achieved in the code implementation for two-dimensional problems – limited only by the machine's capacity to represent numbers. On the other hand, there still is the cost–benefit question – considering that the mathematical governing equations are adequate for representing the physical phenomenon – of how to improve a real problem's simulation without increasing the number of degrees of freedom. The first possibility is to increase the polynomial order of the interpolating functions (p-refinement). The second possibility is with local, adaptive, h-refinement of the discretization mesh. We may also attempt to optimize the geometric location – inside a boundary element – to which the problem's primary parameters are attached. Independently of that, an isoparametric formulation may fail to reproduce the exact geometry of the idealized physical problem. Since, for two-dimensional problems, we have the boundary element formulation under control regarding all numerical evaluations, we assess how an isoparametric analysis – with the introduced elegancy of a convergence theorem – compares to a formulation that preserves the problem's idealized geometry but is not isoparametric, in general. We present the conceptual formulation, code implementation, and numerical illustrations that go from the simple case of an infinite plate with a circular hole to very challenging – physically unrealistic but mathematically conceivable – topological applications.

Keywords: consistent boundary elements, collocation, isoparametric analysis, isogeometric approach, node location optimization, homothetic mesh refinement.

1 INTRODUCTION

Our recent proposition of the 'consistent' collocation boundary element method (CBEM) has required a long maturation time since the primitive proposal [1] of 30 years ago (Here, the word 'primitive' may refer to 'original, primary, crude or rudimentary', but also to 'seminal', as the concept of 'complex singularity poles' – bad marketing but trustful mathematics – was laid down for the first time). Some contributions followed sparsely [2]–[5] until the three-paper publication [6]–[8], which brought the theoretical basis for general linear problems of elastostatics and steady-state potential, with code-implementation and applications for the two-dimensional (2D) case. Although properly using the concept of 'complex singularity poles', these papers were based on real-variable Cartesian coordinates. A fully complex-variable reformulation followed [9], also as the subject of a technical presentation during last year's BEM/MRM conference [10].

Despite the sound mathematics laid down in the papers just outlined, the question 'can we do better?' (for the particular case of 2D linear problems of elastostatics and steady-state potential) persists concerning an efficient numerical simulation:

WIT Transactions on Engineering Sciences, Vol 136, © 2024 WIT Press
www.witpress.com, ISSN 1743-3533 (on-line)
doi:10.2495/BE470011

1. A first issue refers to an eventual optimal node location inside a boundary element.
2. An efficient – problem-dependent – mesh-refinement technique should be considered.
3. Moreover, the isoparametric formulation – and the related, elegant convergence theorem proposed in Dumont [6] for generally curved elements – may require the approximate representation of the problem's boundary geometry, and, then, not be the best one.

We are concerned rather with concepts than with code-implementation aspects and numerical assessments. This contribution is meant as the layout of a paper in preparation [11].

The denomination 'geometry-preserving' is in the present context more informative than and not committed to the term 'isogeometric' proposed by Cottrell et al. [12] for widespread applications also in the frame of the boundary element method – which do not take into account the mathematical consistency of our developments.

Before proceeding with the items above, it is necessary to outline a consistent notation [6]–[9], [13], which was restricted to the isoparametric formulation. The following developments are less formal but perhaps more intuitive, as we first resort to two elasticity applications, taken from Dumont [10], [13] and to be seen not just as a repetition but rather as a motivation and the illustration of how the numerical solution possibilities are deemed to evolve.

2 TWO ILLUSTRATIVE APPLICATIONS

Infinite plate with a hole. Fig. 1 shows on the left an infinite plate with a circular hole of radius a. The displacement and stress solutions for a uniform stress field $\sigma_{xx} = 1$, $\sigma_{yy} = \tau_{xy} = 0$ applied at infinity, according to Sadd [14], for instance, are compactly expressed in polar coordinates as

$$\begin{aligned} u_r &= \frac{1}{4Gr^3}\left[\cos 2\theta\left(4(1-\nu)a^2r^2 + r^4 - a^4\right) + (1-2\nu)r^4 + a^2r^2\right] \\ u_\theta &= \frac{1}{4Gr^3}\sin 2\theta\left[4\nu a^2r^2 - \left(a^2+r^2\right)^2\right] \end{aligned} \tag{1}$$

$$\begin{aligned} \sigma_{rr} &= \frac{1}{2}\left(1-\frac{a^2}{r^2}\right) + \frac{1}{2}\left(1-4\frac{a^2}{r^2}+3\frac{a^4}{r^4}\right)(2\cos^2\theta - 1) \\ \sigma_{\theta\theta} &= \frac{1}{2}\left(1+\frac{a^2}{r^2}\right) - \frac{1}{2}\left(1+3\frac{a^4}{r^4}\right)(2\cos^2\theta - 1) \\ \tau_{r\theta} &= \left(-1-2\frac{a^2}{r^2}+3\frac{a^4}{r^4}\right)\sin\theta\cos\theta \end{aligned} \tag{2}$$

The maximum stress value is $\sigma_{\max} = \sigma_{\theta\theta}(r=a, \theta = \pm\pi/2) = 3$, and we also obtain the highest normal stress in the vertical direction $\sigma_{\theta\theta}(r=a, \theta=0) = -1$.

As indicated on the right in the figure, we discretize the circular cavity with 10 quartic elements and 40 equally spaced, equidistant nodes from the center – not taking advantage of the double symmetry. The main source of errors in this simulation is related to the fact that the circular surface is modeled with quartic polynomial elements, with non-smooth transition between elements. In fact, we measure for nodes 1, 5, 9, 13, 17, 21, 25, 29, 33 and 37 the same lack of smoothness, with $(\theta^+ - \theta^-)/2\pi \approx 0.4999900076$, when it should be exactly $1/2$. Then, we should not expect in our numerical evaluations a relative accuracy error smaller than about 0.00001998. When evaluating results, points along a horizontal axis on the right in Fig. 1 – which goes through nodes 21 and 1 – should present the largest errors, as there is some angularity there. Tangents about nodes 11 and 31 are horizontal and we should expect

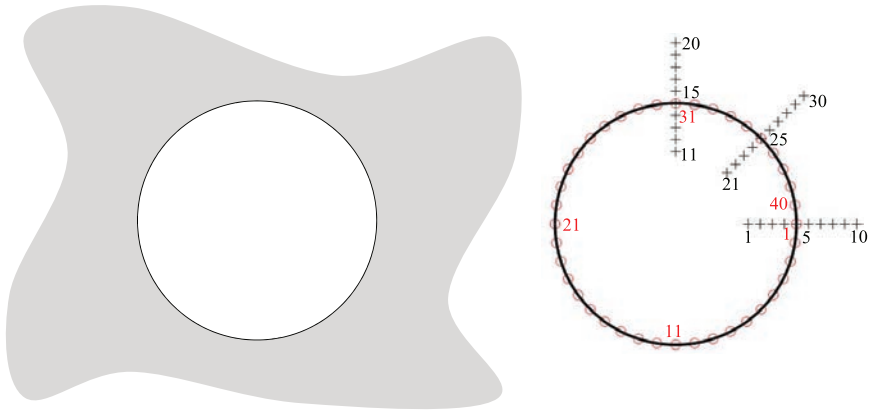

Figure 1: Infinite plate with a circular hole (left) modeled as 10 quartic elements (right) with 30 points at which results are to be evaluated.

the smallest errors measured along a vertical from there. Nodes 6, 16, 26 and 36, which are located at angles multiple of $\pi/4$ of inclination, do not have tangents inclined of exact multiples of $\pi/4$, since they are not middle nodes of the quartic elements. Such lacks of polar symmetry are intentional in order to have geometric simulation errors introduced in our model. The figure also indicates three series of 10 points, each, at which stress results are to be evaluated. Points 1, 11 and 21 are $0.6 + 10^{-10}$ distant from the center, with interpolated points up to the respective points 10, 20 and 30, which are at a distance $1.5 + 10^{-10}$ from the center, in such a way that points 1 ... 4, 11 ... 14 and 21 ... 24 are actually internal to the cavity, that is, external in relation to the open domain of interest. We intentionally set points 5, 15 and 25 inside the open domain and just 10^{-10} distant from the respective nodes 1, 31 and 36. Besides the geometry errors, we should expect some round-off errors related to these close points. This is assessed in Dumont [10], [13] and not repeated here.

The superiority of applying the present geometry-preserving formulation to this kind of problem is numerically demonstrated in Dumont [11].

Topologically extremely challenging problem. Fig. 2 represents a 2D domain (about 25 units across) with some challenging topological features, to be subjected to a series of elastic fields, as described in Dumont [9] and summarized in Dumont [13], which is on the other hand a development of a simpler numerical model proposed in Dumont [8]. Readers are referred to these papers for the complete description of this *cut-out* test and thorough result assessments. The cusp at node 1 has an internal angle of about 10^{-8} *rad*, the external angle at node 17 is of about 10^{-13} *rad*, and the strip of material between the cavity and the external boundary is only about 10^{-4} unities wide, for an isoparametric formulation with quadratic elements. As detailed in Dumont [9], these angles and distances are much larger when we just switch to quartic elements, which makes the geometric problem discretization-dependent: a disadvantage of the isoparametric formulation, to be addressed next.

The indicated crosses in Fig. 2 are a total of 41 – in part internal and in part external – points at which stress results are to be numerically evaluated for the applied stress fields. Some of these points are very close to the boundary, as described and assessed in Dumont [8], [9]. Most important, we generate between internal point 30 and node 69, which are visually indistinguishable from each other in the figure, a series of 10 points that approach node 69 at geometrically decreasing distances, as indicated in the first row of Table 1 of Dumont [9],

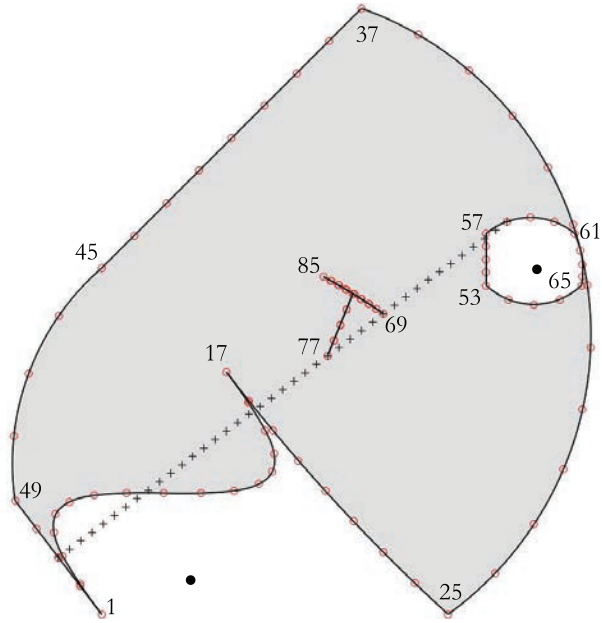

Figure 2: Two-dimensional figure with some challenging topological issues and to be subjected to a series of elastic fields, as reproduced from Dumont [9].

[13]. A similar series of 10 very close points to node 17 is also generated, with the distances indicated in the second row of the mentioned Table: these distances go as small as 10^{-17} and 10^{-18}. If we consider all geometric data given in meters, the smallest distances are actually about one thousandth of a typical proton size, which is meaningless in terms of continuum mechanics but not mathematically!

As indicated in Dumont [13], this elastic body is subjected to two rigid-body translations and a set of four linear, quadratic, cubic, quartic and quintic polynomial fields, thus a total of 22 fundamental (that is, homogeneous) solutions of the elastostatics problem for homogeneous, isotropic material, as given in eqns (15–19) of Dumont [8] in terms of real variables, and very compactly on the right in eqn (34) of Dumont [9], in terms of the complex $z = x + iy$. Rigid-body rotation is obtained as the combination of two of the linear solutions.

The main issue when dealing with such a problem in the frame of an isoparametric formulation is that the challenging geometry is discretization-dependent. Then, distinct meshes reproduce distinct, albeit approximate, problems – and then not strictly comparable.

3 BASIC PROBLEM FORMULATION IN THE CONSISTENT, COLLOCATION BOUNDARY ELEMENT METHOD

The peculiarities of present interest for the evaluation of results at internal points are dealt with in the papers referenced above, and shall not be addressed here.

Whether using real or complex variables, the basic system matrix to be solved in the frame of the CBEM has the format

$$\mathbf{H}(\mathbf{d} - \mathbf{d}^p) = \mathbf{G}(\mathbf{t} - \mathbf{t}^p)_{ad} \tag{3}$$

In this equation, $\mathbf{H}$ is the square, double-layer potential matrix of order $n_d = 2n_n$, for 2D elasticity and the problem discretized with n_n nodal points, and $\mathbf{G}$ is the single-layer potential matrix with $2n_n$ rows and $2(n_n + n_e)$ columns, as we code for n_e elements of any order o_e, in principle taking into account that the left and right tangents at a nodal point connecting two elements are different, in the isoparametric formulation for generally curved boundaries. The number of columns of $\mathbf{G}$ may be significantly smaller in the patch-related, geometry-preserving formulation we are about to present.

As laid down in Dumont [4], [6], we are assuming just for the sake of elegant and compact formulation that some *particular* solution of interest is known – whether or not related to non-zero body forces – and may be approximately expressed as boundary nodal displacement $\mathbf{d}^p$ and traction $\mathbf{t}^p$ data. This is the case of the infinite plate with a hole of Fig. 1 [10], [13]. The problem's primary boundary displacement and traction parameters are $\mathbf{d}$ and $\mathbf{t}$, which are in part known and in part to be obtained in the frame of a general mixed-boundary formulation ($\mathbf{t} = \mathbf{0}$ for the problem of Fig. 1, and $\mathbf{d}$ is to be obtained). As comprehensively assessed in Dumont [3], [6]–[8], we write for consistency that the traction $(\mathbf{t} - \mathbf{t}^p)_{ad}$ is *admissible*, in equilibrium with the applied domain forces: this follows the same mathematical/mechanical principle that, since – for a finite domain – rigid-body displacement amounts of $(\mathbf{d} - \mathbf{d}^p)$ cannot be transformed into forces, also non-equilibrated forces should not be transformed into displacements (see Section 5.3).

In complex-variable, 2D plane-strain elasticity, the matrices of eqn (3) are [9]

$$G_{s\ell} = \int_\Gamma \begin{bmatrix} -(3-4\nu)\,\ln(z\bar{z}) & \dfrac{z}{\bar{z}} \\ \dfrac{\bar{z}}{z} & -(3-4\nu)\,\ln(z\bar{z}) \end{bmatrix} \frac{|J|_{(at\ \ell)} N_\ell^{o_e} \mathrm{d}\xi}{16\pi G\,(1-\nu)} \tag{4}$$

$$H_{sn} = \int_\Gamma \begin{bmatrix} (3-4\nu)\dfrac{z'}{z} - \dfrac{\bar{z}'}{\bar{z}} & \dfrac{z'}{\bar{z}} - \dfrac{z}{\bar{z}^2}\bar{z}' \\ -\dfrac{\bar{z}'}{z} + \dfrac{\bar{z}}{z^2}z' & \dfrac{z'}{z} - (3-4\nu)\dfrac{\bar{z}'}{\bar{z}} \end{bmatrix} \frac{i N_n^{o_e} \mathrm{d}\xi}{8\pi\,(1-\nu)} + \delta_{sn} \tag{5}$$

Real-variable expressions [7] might substitute for the above, but the complex representation is undeniably simpler. Here, $z = x + iy$, and we use $n = -iz'/|J| \Leftrightarrow \bar{n} = i\bar{z}'/|J|$ for the unit normal, also considering $\mathrm{d}\Gamma = |J|\mathrm{d}\xi$. The material's shear modulus and Poisson's ratio are G and ν.

The rows above refer to the *source*, complex point force $p_s^* = (p_x^* + i\ p_y^*)|_{(at\ s)}$ and its conjugate $\bar{p}_s^* = (p_x^* - i\ p_y^*)|_{(at\ s)}$. The first columns stand for either *node* n or *locus* ℓ on a boundary segment, to which either complex displacements $d_n = (d_x + i\,d_y)|_{(at\ n)}$ or tractions $t_\ell = (t_x + i\ t_y)|_{(at\ \ell)}$ are attached.

Only the first rows of the above matrices need to be implemented in a code [9].

We develop eqns (4) and (5) for evaluations using Gauss–Legendre quadrature and then eventually accrue mathematically exact corrections conditioned by three logical constants $< no\_sing,\ sing,\ quasi\_sing >$. This is thoroughly addressed in Dumont [9], [13].

4 CONSISTENT NOTATION AND IMPLEMENTATION POSSIBILITIES

We present the basic notation formally proposed in the previous papers [6], [13], but add the possibility of working with the concept of boundary patches and geometry-preserving description. We resort to the applications of Section 2 to underlie the technical arguments.

Three geometric entities are considered in eqns (4) and (5) for the elasticity problem.

Displacement and traction representation. The real functions $N_n^{o_e} \equiv N_n^{o_e}(\xi)$ and $N_\ell^{o_e} \equiv N_\ell^{o_e}(\xi)$ of the real, natural variable $\xi \in [0,1]$ interpolate displacements and tractions, respectively, along a generic boundary segment $\Gamma_{seg} \equiv \Gamma_{seg}(\xi)$, $\xi \in [0,1]$, of the problem's whole boundary Γ. This is carried out in the frame of a *consistent* formulation, to which the reader is referred in order to fully understand our developments (we maintain that the developments in the textbooks on the BEM are not consistent). The functions $N_n^{o_e}$ interpolate displacements from *nodal* displacements d_n, whereas $N_\ell^{o_e}$ interpolate from traction parameters attached to boundary *loci* (attention to Ansatz 2 and eqn (20) of Dumont [6]!). Observe that *nodes n* and *loci* ℓ are different geometric entities that may be differently allocated along the boundary.

The superscript o_e in both $N_n^{o_e}$ and $N_\ell^{o_e}$ is the interpolation order in terms of Lagrangian polynomials, as we have considered in the previous papers and are considering here. As outlined in Dumont [6], $o_e = 0$ corresponds to the *constant* element and, although implicit in our developments, should be avoided for referring to a superparametric formulation (just use $o_e = 1$ for better results with the same computational effort). Our codes are implemented for the four cases $o_e = 1, 2, 3, 4$, but higher-order elements are seamlessly supported.

Isoparametric boundary geometry description. We also recognize in eqns (4) and (5) the boundary geometry description given by the complex $z \equiv z(\xi) - z_s = x(\xi) - x_s + i\,(y(\xi) - y_s)$, then referred to a *source* point s that may be infinitesimally close to but is conceptually not on the boundary [6]. In an isoparametric formulation, the boundary Cartesian coordinates (x, y) are interpolated along each boundary segment Γ_{seg} in terms of interpolation functions $N_m^{o_e}$ (m refers to key geometric points) that are linear combinations of the displacement interpolation functions $N_n^{o_e}$. However, it may not be the most advisable strategy, in general, as illustrated for the circular hole and the cut-out test of Section 2, for their circular and sinusoidal boundary patches.

Schematic illustration. We illustrate on the left in Fig. 3 – as already advanced in Dumont [13] – the case of two consecutive cubic ($o_e = 3$) boundary elements of a 2D elasticity problem, with $n_m = n_n = 4$ *nodes* for geometry ($\circ$) and displacements ($\odot$), which in this case coincide (as it usually occurs in an isoparametric formulation), and $n_\ell = n_n = 4$ *loci* ($\times$) for tractions, which are not at the element extremities but at distances $\epsilon \to 0$ (we do not say 'discontinuous', which is just a misconception [6]). The *points* ($*$) are for the collocation of the sources s in the domain but at distances $\to 0$ from the nodal points n, in the frame of the CBEM. There are $n^d = n^{el}(n_n - 1) = 3n^{el}$ nodes for a total of n^{el} elements that comprise the complete problem we are simulating with cubic elements. For an elasticity problem implemented in terms of real variables, the double-layer potential matrix $\mathbf{H}$ is square of order $2n^d = 2n^{el}(n_n - 1) = 6n^{el}$, and the single-layer potential matrix $\mathbf{G}$ has the same number of rows but $2n^t = 2n^{el}n_\ell = 8n^{el}$ columns, where n^t is the total number of traction *loci*.

The quest 'isoparametric versus geometry-preserving' boundary description is this paper's core. However, we should first briefly address a related subject, itemized as # 1 in Section 1, which may look promising but is not.

4.1 Attempt to optimize *node* n and *locus* ℓ location inside an isoparametric element

The case on the right in Fig. 3 is almost similar to the previous description, also with $n_m = n_n = 4$ *nodes* for geometry and displacements, but whose locations only coincide at the extremities, since we are now considering the abscissas of a Radau–Lobatto quadrature for

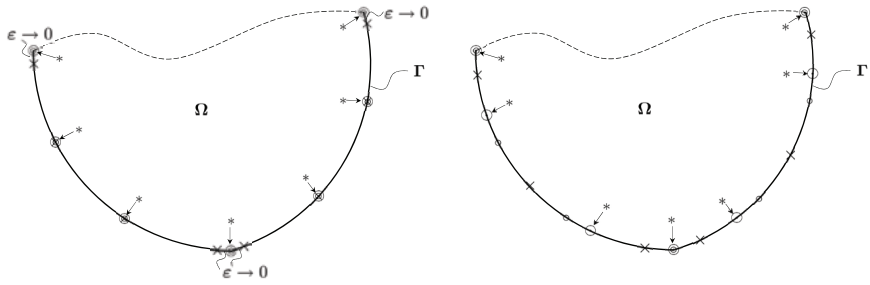

Figure 3: Two consecutive cubic elements for a 2D problem, illustrated on the left for $n_m = n_n = n_\ell = 4$ *nodes* and *loci* per element, and on the right in an optimization attempt for $n_m = n_n = 4$ *nodes* and $n_\ell = 3$ *loci*.

the displacement nodes ($\odot$) while keeping the geometry nodes ($\circ$) unaltered. Most important, we have $n_\ell = n_n - 1 = 3$ parameter *loci* ($\times$) for traction along an element at abscissas given by the roots of a Legendre polynomial, which are at finite distances from the element extremities: such implementation still satisfies the convergence Theorem 1 [6]. There are in this case $n^d = n^t = n^{el}(n_n - 1) = 3n^{el}$ *nodes* and *loci* for a total of n^{el} elements. In terms of real variables, both matrices $\mathbf{G}$ and $\mathbf{H}$ are square of order $2n^d = 2n^{el}(n_n - 1) = 6n^{el}$.

The reason for such an implementation would be to improve the representation capacity of interpolation functions $N_n^{o_e}$ and $N_\ell^{o_e}$, as n_n Radau–Lobatto and n_ℓ Legendre points lead to the accurate integral representation of polynomials of order $2n_n - 3$ and $2n_\ell - 1$, respectively. In the illustrative case of a cubic (order 3) element, we have $2 \times 4 - 3 = 5$ and $2 \times 3 - 1 = 5$, thus 5th (and not just 3rd) order polynomial representations for displacements and tractions.

Such an idea of polynomial optimization seems tempting and may deserve some numerical experimentations (we already have the code implementation). However, there are some issues to consider. First, the polynomials $N_\ell^{o_e}$ and $N_n^{o_e}$ do not feature alone in a boundary element implementation, but rather multiplied with some functions, as given in eqns (4) and (5). Then, the integral representation capacity referred to in the above paragraph – and the basis of the Gauss–Legendre quadrature – does not take place in the applications of interest. A second, not strong reasoning would be in terms of result interpretation, as the n_n and n_ℓ locations are not as simply distributed as in the scheme on the left in Fig. 3. There is, however, a very strong argument against such an optimization attempt, which is related to the lack of smoothness in the distribution of n_n and n_ℓ locations along a boundary patch – particularly in the frame of an adaptive mesh refinement, as we address next.

5 THE CONCEPT OF GEOMETRY-PRESERVING BOUNDARY PATCHES Γ_{patch}

The geometry and all relevant mesh-generation data of the circular hole of Fig. 1 are given in terms of just two semicircles and three lines of data. As given in Table 1 of Dumont [9] and to be observed in Fig. 2, the features of this topologically challenging model require 18 lines of data for complete generation of all 15 boundary patches. (We need an extra line with a dummy node to close a subboundary). The concept of *boundary patch* (Γ_{patch}) leads to a simpler and faster code for the same data entry, as an advancement of the codes reported in our recent publications. In Table 1 of Dumont [9], for instance, the first patch starts at node 1, coordinates $(0, 0)$, and finishes at node 17, coordinates $(7.2, 14)$, with the geometry deviating from the chord $1 - 17$ by the curve $y_{patch}(\zeta) = 5\sin(2\zeta\pi), \zeta \in [0, 1]$. This patch generation

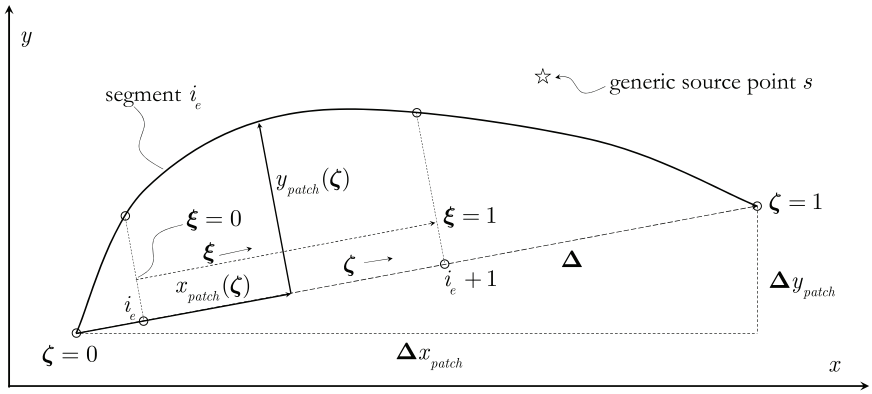

Figure 4: Generic boundary patch $\Gamma_{patch}(\zeta)$, $\zeta \in [0,1]$ with a segment $\Gamma_{seg}(\xi)$, $\xi \in [0,1]$.

is for quartic elements ($o_e = 4$) and 4 elements, which means that the key node number 17 is itself generated (= $1 + o_e \times 4$). We enter for this patch that the distance from node to node varies at a geometric rate $f_{node} = 1.0$, is then constant (increasing and decreasing node distances occur for the patches connecting 17–25 and 61–65).

5.1 Homothetic node and element generation

Fig. 4 represents a general patch that spans from (x_{init}, y_{init}) to (x_{final}, y_{final}) and has the shape $(x_{patch}(\zeta) = \Delta\zeta, y_{patch}(\zeta))$, $\zeta \in [0,1]$ where $y_{patch}(\zeta)$ must be entered.

We may have any topologically consistent boundary shape $y_{patch}(\zeta), \zeta \in [0,1]$, in which 'consistent' means taking care that the Jacobian of the coordinate transformation keeps positive not only along the curved boundary but also in the complex vicinity, such as for the indicated source point s, for the analytical corrections of eventual quasi singularities [6]–[9], [13] to take place. Once the patch-referred coordinates are obtained, the global coordinates become, here expressed in terms of the complex $z(\zeta) = x(\zeta) + iy(\zeta)$, for simplicity,

$$z(\zeta) = z_{init} + z_{patch}(\zeta)\frac{\Delta z_{patch}}{\Delta} \tag{6}$$

In our previous codes, the outer-most loop spans all boundary elements (segments Γ_{seg}), as shown in Algorithm 1 of Dumont [6], for (computationally more involved) geometric data should be evaluated first. We are coherently proposing that the outer-most loop runs for the boundary patches, $i_{patch} = 1 \ldots n_{patch}$, with geometry pre-evaluations carried out and stored for a typical element of the patch, as shown next (see also [11]), which includes adaptive mesh refinement along a patch within the concept of *homothetic elements*. (We might have element orders o_e differing from patch to patch.) Only then we run a loop for the source points s, evaluate the patch-related complex distance ζ_s, and then the loop for all elements inside the patch, again, for which the pre-evaluations have been done.

Fig. 5 is the schematic illustration of how homothetic elements are generated, with four meshes going from node 1 through node 13, for the generation of 12 linear, 6 quadratic, 4 cubic or 3 quartic elements including eventual internal natural points $\xi_j, j = 2 \ldots o_e$, as we always have $\xi_1 = 0$ and $\xi_{o_e+1} = 1$.

In this figure, the nodes 2 to 12 are generated in such a way that the distance between consecutive nodes increases at a geometric rate $f_{node} = 1.25$. In our homothetic element

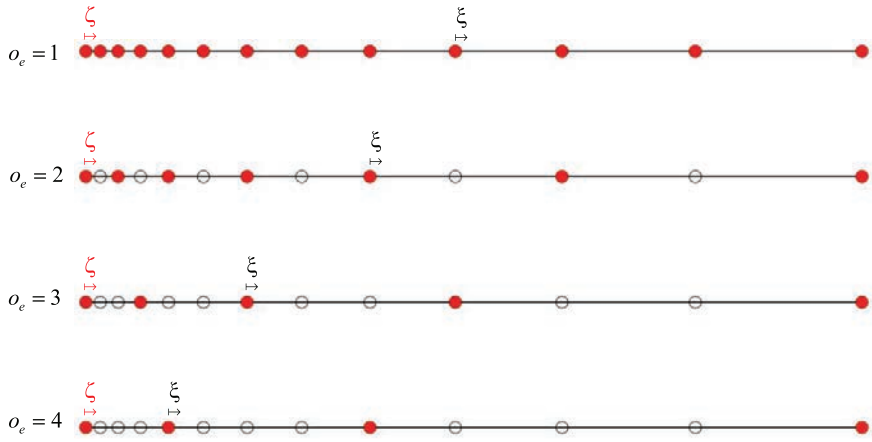

Figure 5: Schematic representation of a boundary patch (natural coordinate $\zeta \in [0, 1]$) with 13 nodes (circles), whose consecutive distances grow at the rate $f_{node} = 1.25$. The homothetic subdivision for linear through quartic elements (natural coordinates $\xi_j \in [0, 1]$, solid circles for the respective end nodes) is also indicated.

generation, the relative size f_{el} of consecutive elements also increases exponentially:

$$f_{el} = f_{node}^{o_e} \tag{7}$$

This means that the node locations inside any element of the patch have the same representation in terms of the element natural coordinate $\xi \in [0, 1]$, which is illustratively shown for some elements in the figure. This is the reason of calling 'homothetic' such combined element and node generation. Given a boundary patch i_{patch}, we first carry out all necessary geometric and singularity-related pre-evaluations for a representative element of the patch and only then proceed with the algorithm that takes the source points into account. These pre-evaluations include the analytical expression and storage of $N_n^{o_e}$ and $N_\ell^{o_e}$ as well as of the integrals required in the quasi-singularity corrections – always taking into account that the natural node coordinates $\xi_j, j = 1 \ldots o_e + 1$ are not equally spaced inside the element but rather reflect the distance amplification illustrated in Fig. 5. This means, for instance, that the Jacobian for coordinate transformations along straight and circular patches is constant, which leads to smaller quadrature errors. (See the second paragraph of Section 5.1.)

Let n_ζ be the numbering difference between the first and last nodes of a patch ($n_\zeta = 13 - 1 = 12$ in Fig. 5). We set

$$\tilde{\zeta} = 1 \Big/ \sum_{j=0}^{n_\zeta - 1} f_{node}^j \,, \quad \delta = 0 \tag{8}$$

and carry out the simple algorithm for the evaluation of the local ζ_i coordinates of the generated nodes in the patch:

$$\begin{aligned} &\text{for } i \text{ from 1 to } n_\zeta + 1 \text{ do} \\ &\quad \zeta_i = \delta \tilde{\zeta} \\ &\quad \delta \leftarrow \delta f_{node} + 1 \\ &\text{end do} \end{aligned} \tag{9}$$

The coordinate transformation between patch coordinate ζ and element coordinate ξ is given for the i_th element, according to Fig. 5, as

$$\zeta = \zeta_i + \xi\,(\zeta_{i+1} - \zeta_i) \quad \Leftrightarrow \quad \xi = (\zeta - \zeta_i)/(\zeta_{i+1} - \zeta_i), \quad \zeta \in [\zeta_i, \zeta_{i+1}] \tag{10}$$

and the Jacobian of the coordinate transformation is

$$|J(\xi)|_{seg} = |J(\zeta)|_{patch} \left.\frac{\partial \zeta}{\partial \xi}\right|_{seg} = |J(\zeta)|_{patch}\,(\zeta_{i+1} - \zeta_i)\,, \quad \zeta \in [\zeta_i, \zeta_{i+1}] \tag{11}$$

with, in complex coordinates, $|J(\zeta)| \equiv |\partial z(\zeta)/\partial \zeta|$.

5.2 Evaluation of the complex ζ_s coordinate of a quasi-singular point source $z_s = x_s + iy_s$

Fig. 4 depicts a *star* for a generic source point. Such points are also indicated as *crosses* (+) in Figs 1 and 2, and may be extremely close to the boundary, as illustrated in Section 2 with reference to Dumont [6]–[9], [13]. In these papers, the complex natural coordinate ξ_s corresponding to a close source point $z_s = x_s + iy_s$ is evaluated iteratively for every boundary segment Γ_{seg}, as its geometry is given – in the frame of an isoparametric formulation – piecewise in terms of the interpolation functions $N_n^{o_e}(\xi)$ with local support $\xi \in [0, 1]$. In the present geometry-preserving formulation, we have a unique analytical function $z(\zeta)$ spanning a whole boundary patch, according to eqn (6). The search is then for the patch-related complex natural coordinate ζ_s in terms of the same Newton–Raphson algorithm outlined in Appendix A of Dumont [6]. Once obtained for a given patch $\Gamma_{patch}(\zeta)$, ζ_s is successively transformed into the complex ξ_s for each one of the boundary segments $\Gamma_{seg}(\xi)$ according to the same eqn (10):

$$\xi_s = (\zeta_s - \zeta_i)/(\zeta_{i+1} - \zeta_i), \quad \text{for the i\_}th \text{ boundary segment} \tag{12}$$

where both ζ_s and ξ_s are in general complex. When the boundary patch is either a straight segment or an arc of circle, as in Fig. 1 or in 14 of the 15 patches of Fig. 2, the natural coordinates ζ and ξ of the general Fig. 4 are defined as following along the curved patch, leading to a constant Jacobian even for adaptive mesh refinement. In such particular cases, the complex source point ζ_s may be obtained analytically, which speeds up calculations [11].

5.3 Spaces **W**, **R** of inadmissible displacements and tractions

Rigid-body displacements. We have proposed at the very beginning of our developments on boundary element methods [15] a matrix **W** as the basis of rigid-body displacements in a finite domain, as expressed for elasticity. This is shown in detail in Dumont [6], where it is set in eqn (18) of **Definition 1** that the rigid-body displacements u_{ik}^r along the boundary are linear combinations of the displacements $N_n^{o_e}$. However, this only holds in the isoparametric formulation. In the present geometry-preserving context for 2D problems, the three rigid-body displacements (two translations and one rotation) at a given point of the boundary are

$$\begin{bmatrix} u_1^r & u_2^r & u_3^r \\ \bar{u}_1^r & \bar{u}_2^r & \bar{u}_3^r \end{bmatrix} \Leftarrow \begin{bmatrix} 1 & i & iz(\zeta) \\ 1 & -i & -i\bar{z}(\zeta) \end{bmatrix} \quad \text{at a point of the boundary patch} \tag{13}$$

here defined in terms of the complex variable, so that we only evaluate the first matrix row.

Inadmissible tractions. Building up on a 1998 paper [3], it is shown in Dumont [6] – and explored subsequently also in the context of complex variables [9], [13] – that a *consistent* boundary element formulation requires that, for a finite body, if the rigid-body amount of displacements $(\mathbf{d} - \mathbf{d}^p)$ in eqn (3) cannot be transformed into forces, conversely, the amount of non-equilibrated tractions $(\mathbf{t} - \mathbf{t}^p)$ cannot be transformed into displacements:

$$\mathbf{HW} = \mathbf{0} \quad \Leftrightarrow \quad \mathbf{G}_{ad}\mathbf{R} = \mathbf{0} \tag{14}$$

This reasoning leads to the evaluation of the rigid-body displacement amount in the expression of a fundamental solution, embedded in the single-layer potential matrix $\mathbf{G}_{ad}$, where the subscript means the filtered, *admissible* part of the matrix. The reader is referred to Dumont [6], where the matter is illustrated didactically. The formulation in terms of a complex variable is shown in Appendix A.2.2 of Dumont [9]. In the case of a geometry-preserving formulation,

$$R_{\ell k} = |J|_{(\text{at } \ell)} \int_0^1 \begin{bmatrix} 1 & i & iz\,(\zeta(\xi)) \\ 1 & -i & -i\bar{z}\,(\zeta(\xi)) \end{bmatrix} N_\ell^{o_e}(\xi)\mathrm{d}\xi \quad \text{for a boundary element} \tag{15}$$

obtained using Gauss–Legendre quadrature along each segment of the whole boundary, as $N_\ell^{o_e}$ has local support for $\xi \in [0, 1]$ [6], [9], [11], [13].

The left part of eqn (14) is rather axiomatic also in the present context and has been checked numerically for the topologically challenging example of Fig. 2: errors are only due to the Gauss–Legendre quadrature of the problem's regular integrals.

6 CONCLUDING REMARKS

The developments proposed in Dumont [9], [10] as the complex-variable counterpart of Dumont [6]–[8] for 2D potential and elasticity problems could be further improved, as shown in this short contribution and to be thoroughly assessed in a paper in preparation [11]. Further to properly addressing the three entities – *boundary nodes n* (for potentials or displacements), *boundary loci* ℓ (to which normal fluxes or tractions are referred), and *domain points s*, at which we collocate the singular sources in the context of an isoparametric formulation – we show that a *geometry-preserving* concept must be explicitly resorted to if numerical precision and accuracy are deemed relevant in the numerical simulation of real-world problems. The convergence Theorem proposed in Dumont [6] is no longer applicable but this seems to be compensated by the attained geometric description of a physical model – particularly when dealing with topologically challenging configurations.

We use the concept of *geometry-preserving boundary patches* Γ_{patch}, along which boundary nodes and elements are adaptively refined in a *homothetic* concept. This avoids distortions in the problem's geometry description and leads to more robust simulations and more accurate and reliable results, as assessed in Dumont [11]. Given a source point (x_s, y_s), we only need to evaluate its complex location ζ_s once for a whole boundary patch Γ_{patch}. This and the simplifications related to the *homothetic* mesh refinement, particularly using the complex $z = x + iy$, lead to the assembling time of all relevant matrices significantly smaller than in the original code. The analytical, correction terms to be accrued for quasi-singularities are the same ones previously proposed.

ACKNOWLEDGEMENTS

This project was supported by the Brazilian federal agencies CAPES and CNPq, as well as by the state agency FAPERJ.

REFERENCES

[1] Dumont, N.A., On the efficient numerical evaluation of integrals with complex singularity poles. *Engineering Analysis with Boundary Elements*, **13**, pp. 155–168, 1994.
[2] Dumont, N.A. & Noronha, M., A simple, accurate scheme for the numerical evaluation of integrals with complex singularity poles. *Computational Mechanics*, **22**(1), pp. 42–49, 1998.
[3] Dumont, N.A., An assessment of the spectral properties of the matrix G used in the boundary element methods. *Computational Mechanics*, **22**(1), pp. 32–41, 1998.
[4] Dumont, N.A., The boundary element method revisited. *WIT Transactions on Modelling and Simulation*, vol. 50, WIT Press: Southampton and Boston, pp. 227–238, 2010.
[5] Dumont, N.A., The collocation boundary element method revisited: Perfect code for 2D problems. *International Journal of Computational Methods and Experimental Measurements*, **6**(6), pp. 965–975, 2018.
[6] Dumont, N.A., The consistent boundary element method for potential and elasticity: Part I – Formulation and convergence theorem. *EABE – Engineering Analysis with Boundary Element Methods*, **149**, pp. 127–142, 2023.
[7] Dumont, N.A., The consistent boundary element method for potential and elasticity: Part II – Machine-precision numerical evaluations for 2D problems. *EABE – Engineering Analysis with Boundary Element Methods*, **149**, pp. 92–111, 2023.
[8] Dumont, N.A., The consistent boundary element method for potential and elasticity: Part III – Topologically challenging numerical assessments for 2D problems. *EABE – Engineering Analysis with Boundary Element Methods*, **151**, pp. 548–564, 2023.
[9] Dumont, N.A., Complex-variable, high-precision formulation of the consistent boundary element method for 2D potential and elasticity problems. *EABE – Engineering Analysis with Boundary Element Methods*, **152**, pp. 552–574, 2023.
[10] Dumont, N.A., Real- and complex-variable implementations of the consistent boundary element method in two-dimensional elasticity: A comparative assessment. *WIT Transactions on Engineering Sciences*, vol. 135, WIT Press: Southampton and Boston, pp. 55–66, 2023.
[11] Dumont, N.A., Consistent boundary element method for two-dimensional problems with geometry-preserving, homothetic element generation. *EABE – Engineering Analysis with Boundary Element Methods*, 2024. To be submitted.
[12] Cottrell, J.A., Hughes, T.J.R. & Bazilevs, Y., *Isogeometric Analysis: Toward Integration of CAD and FEA*. John Wiley and Sons, 2009.
[13] Dumont, N.A., Consistency, precision, and accuracy assessment of the collocation boundary element method for two-dimensional problems of potential and elasticity. *Archive of Applied Mechanics*, **9**, 2024.
[14] Sadd, M.H., *Elasticity, Theory, Applications, and Numerics*, Elsevier, 2005.
[15] Dumont, N.A., The hybrid boundary element method: an alliance between mechanical consistency and simplicity. *Applied Mechanics Reviews*, **42**(11), pp. S54–S63, 1989.